Interface Controlled Oxidation States in Layered Cobalt Oxide Nanoislands on Gold

Alex S. Walton,[†] Jakob Fester,[†] Michal Bajdich,[‡] Mohammad A. Arman,[§] Jacek Osiecki,[⊥] Jan Knudsen,[§,⊥] Aleksandra Vojvodic,[‡] and Jeppe V. Lauritsen*[,†]

[†]Interdisciplinary Nanoscience Center (iNANO), Aarhus University, 8000 Aarhus C, Denmark, [‡]SUNCAT Center for Interface Science and Catalysis, SLAC National Accelerator Laboratory, 2575 San Hill Road, Menlo Park, California 94025, United States, [§]Division of Synchrotron Radiation Research, Department of Physics, Lund University, 221 00 Lund, Sweden, and [⊥]MAX IV Laboratory, Lund University, 221 00 Lund, Sweden

ABSTRACT Layered cobalt oxides have been shown to be highly active catalysts for the oxygen evolution reaction (OER; half of the catalytic "water splitting" reaction), particularly when promoted with gold. However, the surface chemistry of cobalt oxides and in particular the nature of the synergistic effect of gold contact are only understood on a rudimentary level, which at present prevents further exploration. We have synthesized a model system of flat, layered cobalt oxide nanoislands supported on a single crystal gold (111) substrate. By using a combination of atom-resolved scanning tunneling microscopy, X-ray photoelectron and absorption spectroscopies and density functional theory calculations, we provide a detailed analysis of the relationship between the atomic-scale structure of the nanoislands, Co oxidation states and substrate induced charge transfer effects in response to the synthesis oxygen pressure. We reveal that conversion from Co^{2+} to Co^{3+} can occur by a facile incorporation of oxygen at the interface between the nanoisland and gold, changing the islands from a Co—O bilayer to an O—Co—O trilayer. The O—Co—O trilayer islands have the structure of a single layer of β-CoOOH, proposed to be the active phase for the OER, making this system a valuable model in understanding of the active sites for OER. The Co oxides adopt related island morphologies without significant structural reorganization, and our results directly demonstrate that nanosized Co oxide islands have a much higher structural flexibility than could be predicted from bulk properties. Furthermore, it is clear that the gold/nanoparticle interface has a profound effect on the structure of the nanoislands, suggesting a possible promotion mechanism.

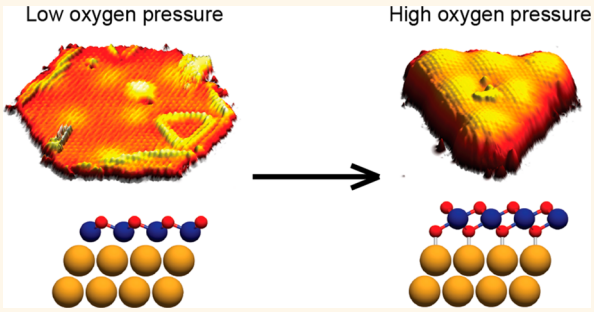

KEYWORDS: water splitting · electrocatalysis · nanocatalysis · cobalt oxide · two-dimensional materials · reducible metal oxides

Electrochemical water splitting is a highly promising new technology for the production of clean, renewable fuel. However, in order to be commercially viable, efficient catalysts are needed for the two half reactions: oxygen evolution (OER) and hydrogen evolution. The OER is a particular challenge, with few materials showing significant activity for this reaction, the majority of which are noble metal oxides. Cobalt oxide is one of the few non-noble metal oxides which shows significant catalytic activity for water oxidation in alkaline solution.[1,2] A key barrier to development of better OER catalysts is a lack of understanding of the surface chemistry of the active phase for OER. Cobalt can form several oxides, containing different formal cobalt valencies and coordinations, leading to large differences in activity. In previous reports of OER, the starting material is often the spinel Co_3O_4 phase, displaying complex surfaces exposing tetrahedrally coordinated Co^{2+} and octahedrally coordinated Co^{3+} species. However, it has been recently revealed that the active phase in electrochemical water oxidation is in fact so-called β-CoOOH, consisting of O—Co—O layers with intercalated hydrogen, where the edges are the active sites for the OER.[3−6] Creating model systems which mimic the properties of this phase and using these models to search for the active sites of these materials is crucial for the rational design of cobalt oxide OER catalysts. It has also been reported that there are synergistic effects

* Address correspondence to jvang@inano.au.dk.

Received for review July 29, 2014 and accepted February 18, 2015.

Published online February 18, 2015
10.1021/acsnano.5b00158

between gold and cobalt oxide, with the presence of a gold/cobalt oxide interface greatly enhancing OER activity;[5,7] however, no consensus has been reached on a mechanism for this effect. Furthermore, the detailed structure of cobalt oxide particles on the nanoscale is known to influence activity, but the role of nanoparticle edges and atomic defects, which often control catalytic activity, have also not been explored.

In this study, we synthesized cobalt oxide nanoislands on a single crystal surface, Au(111), by physical vapor deposition of cobalt in an oxygen environment and subsequent annealing in the same environment. This method allowed us to systematically investigate the structure and composition of the nanoislands as a function of oxygen pressure and temperature using a powerful combination of scanning tunneling microscopy (STM) (for direct, real space imaging of the structure) and X-ray photoelectron and absorption spectroscopies (XPS and XAS) (providing information about the composition, oxidation states and surface chemistry of the nanoislands). To further our understanding at the atomic level, thin films of cobalt oxide supported on Au(111) were modeled using density functional theory (DFT).

Gold was chosen as substrate here so that we could explore the synergistic Au/cobalt oxide interaction and its implications for the catalytic behavior of the resultant nanoislands. Gold is also an excellent substrate for model catalyst studies as (non-nanostructured) gold is catalytically inert, allowing the catalytic properties of the islands and the gold/island interface to be easily determined in future studies. The (111) surface was chosen as the "herringbone" reconstruction facilitates the creation of well-dispersed nanoislands by providing a regular array of nucleation sites for Co.[8,9] Thin films of cobalt oxide on Ir(100) crystals have been extensively studied,[10−12] cobalt oxide has also been investigated on Pd(100)[13] and Pt(111)[14] and there have been some investigations into cobalt oxide on Au(111),[15−17] but to date no analysis of atomic-scale structure of cobalt oxide nanoislands as a function of oxygen pressure has been carried out.

The key finding from our work is that the synthesized Co oxide islands on gold are remarkably structurally flexible during an increase in the formal oxidation state from Co^{2+} to Co^{3+}. As the synthesis oxygen pressure is increased, the structure of the islands changes from a Co−O bilayer with 2+ cobalt to an O−Co−O trilayer with 3+ cobalt, the same structure as a single layer of β-CoOOH. We propose that this structure is stabilized due to charge transfer from the gold to the nanoislands. We propose this will be of great interest as a model system in the search for the active sites of cobalt oxide-based OER catalysts.

RESULTS AND DISCUSSION

Our synthesis procedure consisted of electron beam evaporation of cobalt onto the Au(111) surface in an oxygen environment and a postanneal of the crystal in the same oxygen pressure. We have explored the synthesis procedure for different postanneal temperatures and oxygen pressures. The best synthesis procedure was found for a postanneal temperature fixed at 523 K, and all syntheses at this temperature produced well-dispersed, crystalline nanoislands of cobalt oxide located on the terraces of the Au(111) surface. Postanneal temperatures lower than 473 K were observed to be insufficient to produce crystalline nanoislands and those above 673 K caused coalescence of the nanoislands into large, poorly crystalline structures. Between these two temperatures, there was no obvious temperature dependence on the nanoisland morphology. In contrast, the oxygen pressure during synthesis had a dramatic effect on the nanoisland morphology, with abrupt structural changes observed within a narrow range of oxygen partial pressures. The strongest effect is seen between two pressure regimes, "low" oxygen pressure (1×10^{-6} mbar) and "high" oxygen pressure (1×10^{-5} mbar).

Low Oxygen Pressure: Stoichiometric CoO Islands. At the low oxygen pressure (1×10^{-6} mbar), the surface is covered with atomically flat, 5−10 nm wide nanoislands with two distinct apparent heights (1.7 ± 0.2 Å or 4.0 ± 0.2 Å) and appearances (Figure 1a). Hereafter these will be referred to as Type A and Type B islands, respectively. Both nanoisland types show a truncated hexagonal morphology. Figure 1b,c show atomic resolution STM images of both types of nanoisland and reveal that the surface atoms are arranged in a regular lattice with hexagonal symmetry. As both stable bulk phases of cobalt oxide (CoO and Co_3O_4) have a cubic unit cell, the hexagonal packing of the surface atoms is only compatible with a (111) surface. Measurements of the interatomic spacing on both types of islands show a periodicity of 3.3 ± 0.1 Å with no significant distortion within the basal plane and no dependence on the crystallographic orientation. This surface periodicity is inconsistent with a spinel $Co_3O_4(111)$ surface. The $Co_3O_4(111)$ surface can display a variety of terminations, but only one of the bulk truncated surfaces results in a regular hexagonal periodicity, the Co^{2+} terminated surface. However, the periodicity of the Co^{2+} surface is 5.7 Å,[18] far larger than our observed periodicity. The other spinel surfaces display a kagome lattice structure (Co^{3+} terminated) or a significantly distorted hexagonal structure (O terminated).[19] The observed surface periodicity is closer to the expected spacing for the rocksalt CoO(111) surface, which displays a regular hexagonal lattice with a 3.02 Å periodicity in the close packed directions. Moreover, the difference in apparent heights between the two particle types is 2.3 ± 0.2 Å which is similar to the repeat unit distance between (111) layers in rocksalt CoO(111), 2.46 Å, but far too small for $Co_3O_4(111)$ (4.67 Å).[18] At this point it is

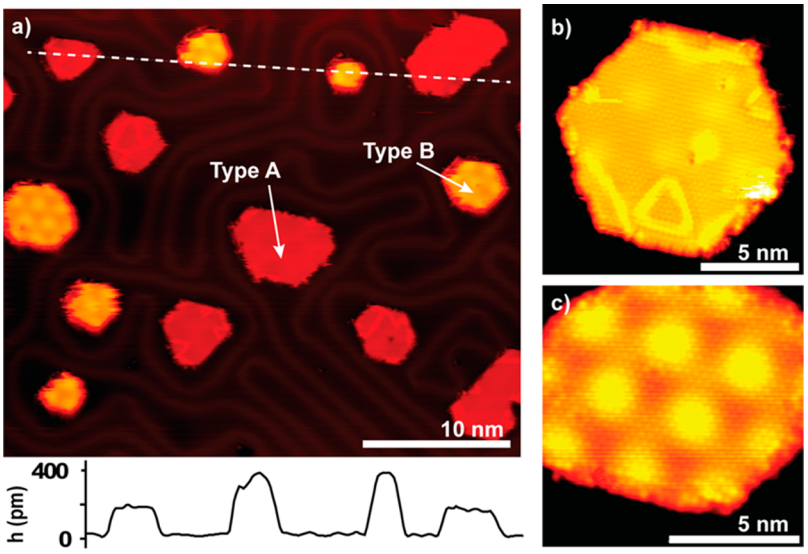

Figure 1. Cobalt oxide nanoislands on Au(111) synthesized at 1×10^{-6} mbar oxygen pressure. (a) Large scale STM image showing distribution and morphology of Type A and Type B nanoislands and different nanoisland types ($V = -558$ mV, $I = 0.36$ nA). Graph shows an apparent height profile along the dotted line. (b) Zoomed-in atom-resolved STM image of a Type A nanoisland ($V = -386$ mV, $I = 0.50$ nA). (c) Zoomed-in atom-resolved STM image of a Type B nanoisland ($V = -174$ mV, $I = 0.70$ nA).

important to emphasize that care should be used when using apparent heights of features measured in STM as the STM image is a convolution of topographic and electronic effects.[20] When measuring the height difference between two dissimilar materials (Au and cobalt oxide in this case) significant deviations from real heights can be observed. However, the height difference between the two types of nanoisland (as they are both cobalt oxide) should be less strongly affected by electronic contributions and therefore closer to a real height difference. It was found that the apparent height of the nanoislands was essentially bias independent at biases < -750 mV, and all reported apparent height measurements were taken in this bias independent regime. Previous STM investigations of thick Co_3O_4 films demonstrate a 5.7 Å in plane periodicity and a 4.67 Å minimum step height.[18] We therefore conclude that the Type A and B structures are single and double layer CoO(111)-like islands, respectively, although with a significant relaxation of the surface in-plane atomic spacing.

A striking feature common to both types of nanoisland is a regular array of diffuse protrusions with the same hexagonal symmetry as the surface atoms (see Figure 1b,c) but much longer range periodicity. This is a moiré pattern formed from overlaying and/or rotating two dissimilar lattices, seen on many other heteroepitaxial films.[11,12,21,22] It differs between the two particle types. In the Type A islands, it has a periodicity of $\lambda_{typeA} = 37 \pm 2$ Å and displays a slight rotation with respect to the atomic lattice of $\theta_{typeA} = 8 \pm 2°$. The moiré corrugation is weak and only just visible over the corrugation due to the surface atoms (0.11 ± 0.02 Å). In the Type B the moiré periodicity is shorter, ($\lambda_{typeB} = 31 \pm 2$ Å) and no rotation is observed between the moiré pattern and the atomic lattice $\theta_{typeB} = 0°$. Here, the moiré corrugation is much stronger (0.28 ± 0.03 Å). The reduction in moiré periodicity between Type A and B islands could reflect a slight expansion of the in-plane lattice constant between Type A and B which our measurements are not precise enough to detect.

Expansion of the in-plane lattice constant of ultrathin heteroepitaxial oxide films relative to bulk values is a commonly observed phenomenon, occurring with, for example, FeO, CoO and ZnO on various substrates.[14,23,24] A common interpretation is that this reduces the surface dipole by moving the oppositely charged metal and oxygen layers closer together, necessitating an in-plane expansion. It should be mentioned that nanoscale cobalt oxide can also adopt the wurtzite crystal structure[25] and that thicker rocksalt CoO films are found to be terminated with a pseudomorphic wurtzite layer.[26] This is also believed to compensate surface polarity as the Co−O spacing can be much closer in wurtzite than in rocksalt.[14]

Taking into account the observations regarding the apparent height and interatomic periodicity of the top layer for the Type A and B islands, we propose the following model for the islands' structure: the Type A consist of one bilayer (*i.e.*, one Co−O unit) of rocksalt CoO(111) with a significantly expanded lattice constant of 3.3 ± 0.1 Å. The Type B are higher and therefore are interpreted as double bilayer islands (two Co−O units). The change in moiré periodicity and apparent moiré corrugation are indicators of both structural and electronic changes within the island, so we propose that the thicker Type B films are in fact wurtzite rather than rocksalt structure (with tetrahedral cobalt coordination rather than octahedral) in accordance with recent observations of two-layer CoO on both Pt(111) and Ir(001).[14,27] Ball

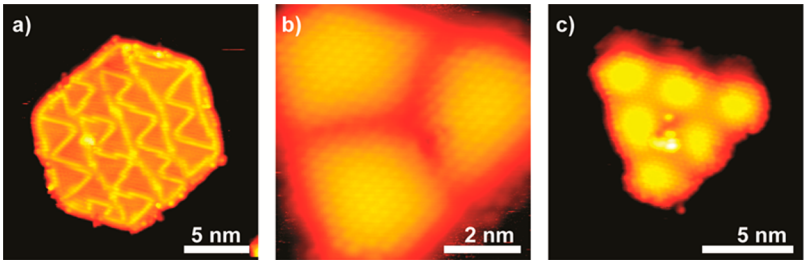

Figure 2. Cobalt oxide nanoislands synthesized at 1 × 10^{-5} mbar oxygen pressure. (a) High defect density Type A particle (−508 mV 0.41 nA). (b,c) Type C islands in atomic resolution (−321 mV, 0.53 nA, −691 mV, 0.40 nA).

models of the proposed Type A and B structures are shown in Figure 3a,b. Detailed first-principle calculations of these and additional structures are performed to test our hypothesis, see discussion below.

A further noteworthy difference between the two particle types is that Type A nanoislands also possess a low density of linear features (Figure 1b) not seen in the Type B islands. We interpret these as oxygen adatom line dislocations as observed in FeO ultrathin films, which form as a result of an additional strain release mechanism.[28] The structure and dynamics of the line dislocations will be discussed in detail in a forthcoming publication.

High Oxygen Pressure: Oxygen Rich Islands. Increasing the oxygen pressure during synthesis to 1 × 10^{-5} mbar caused large changes in the resultant islands which restructure in order to accommodate more oxygen. Type A nanoislands with a high density of linear features were still present in small numbers (Figure 2a), but a third distinct nanoisland morphology is now the majority structure present (Type C, see Figure 2b,c). The Type C islands had an apparent height in between that of the Type A and B islands of 2.9 ± 0.2 Å. There were also a small number of islands with the same morphology as Type C but a significantly larger apparent height of 5 ± 0.2 Å. The surface of the Type C islands was extremely corrugated, even more so than the Type B islands (0.59 ± 0.07 Å). The interatomic spacing was the same as the Type A and B nanoislands (3.3 ± 0.1 Å). The moiré corrugation was less regular than in the Type A and B islands, often appearing distorted, particularly in smaller islands, but had the same periodicity and rotation as the Type B nanoislands. Similar cobalt oxide structures were recently observed on Au(111) and proposed to be spinel Co_3O_4.[17] However, as our atom-resolved images reveal the Type C islands have the same interatomic periodicity and symmetry as the Type A and B structures, they are incompatible with any surface of spinel Co_3O_4 as discussed earlier.

Instead, these islands closely resemble structures that have been observed at high oxygen pressure in FeO films on Pt and Pd(111)[28,29] which also show extremely strong moiré corrugation. In these works, such structures were explained as FeO_2 trilayers, *i.e.*, an extra layer of oxygen exists between the support and the Fe layer. Given the similarities between Fe and Co oxides and the increase in oxygen chemical potential, we propose that the Type C nanoislands consist of a O−Co−O trilayer with the rocksalt structure. The higher islands observed are therefore interpreted as an O−Co−O trilayer with an extra bilayer of Co−O on top (analogous to the Type B structures observed at lower pressures). The effect of increased oxygen chemical potential is therefore the incorporation of an extra layer of oxygen atoms between the Au and the first cobalt layer of the nanoislands, which increases the nominal oxidation state of Co with almost no structural change to the islands. Figure 3c shows a cross-sectional ball model of the proposed Type C island structure. In previous reports of the formation of FeO_2, very high chemical potential of oxygen is required, either by using atomic oxygen[28] or very high oxygen pressures in the mbar regime.[29] Our CoO_2 trilayer islands form at a much lower pressure. This could suggest that oxygen intercalation is much easier than in the FeO/Pt system.

DFT Simulations of Ultrathin Cobalt Oxide Layers on Au. We performed density functional theory (DFT) simulations to elucidate the atomic structure of the different experimentally observed supported CoO_x nanoislands under different oxygen pressure. Surface structural models of the nanoislands were constructed as infinite thin CoO_x films on-top of three layers of Au(111), using the equilibrium lattice constant of Au (a_{lat} = 4.157 Å, see also Supporting Information). These structural models are used as a first order approximation of the nanoislands as they are able to capture the stability order between overlayers with different structures, various Co to O stackings and Co−O bonding coordination, different terminations and CoO_x/Au interfaces. Figure 3 shows the structural models, some of which are proposed based on experimental findings as discussed above. The different considered films consisted of 1 ML of rock-salt (RS) CoO (Type A) (a), 2 ML of wurtzite (WZ) CoO (Type B) (b) and 1 ML of RS CoO_2 (Type C) (c) with extra oxygen layer compared to (a). Additionally, we have also tested the stability of 2 ML spinel Co_3O_4 structures, interfaced to gold *via* either Co (d) or *via* oxygen (e) as well as the stability of 1 ML Co_2O_3 in a k-phase arrangement (f).[30] The proposed structures reflect both types of metal−oxygen bonding: purely octahedral (a) and (c), and purely tetrahedral type (b). The spinel type structures (d) and (e) have both types of bonding.

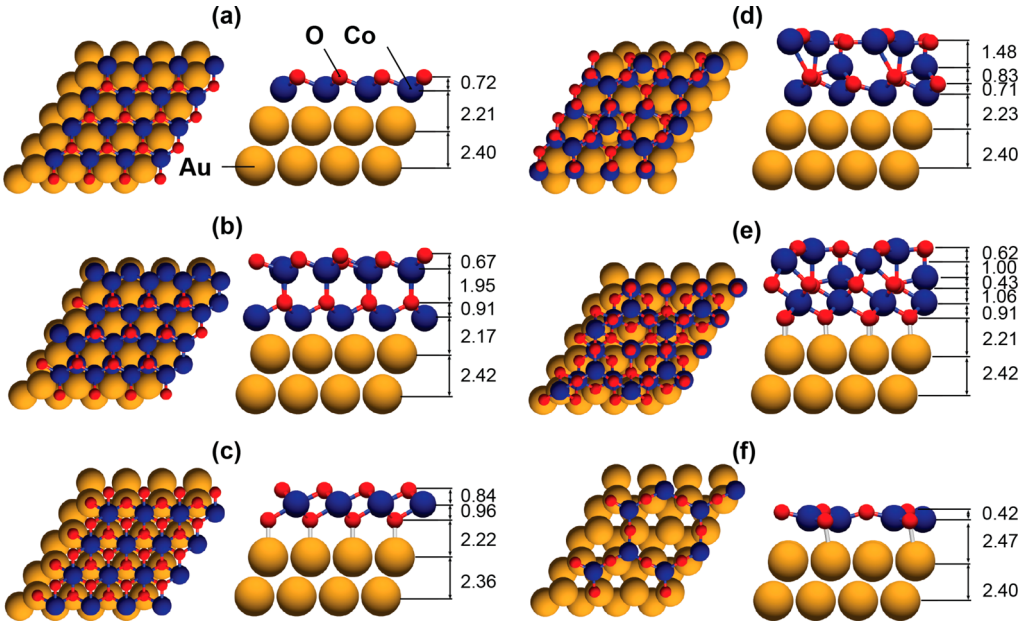

Figure 3. Atomic representation of different CoO_x films adsorbed on the Au(111) surface. (a) Type A structure with 1 ML of RS CoO. (b) Type B structure with 2 ML of WZ CoO. (c) Type C structure with CoO_2 stoichiometry. (d) 2 ML of spinel Co_3O_4. (e) Same as (d) but with extra oxygen layer near Au. (f) 1 ML of Co_2O_3 in a k-phase arrangement.[30] The labels indicate distances in Å.

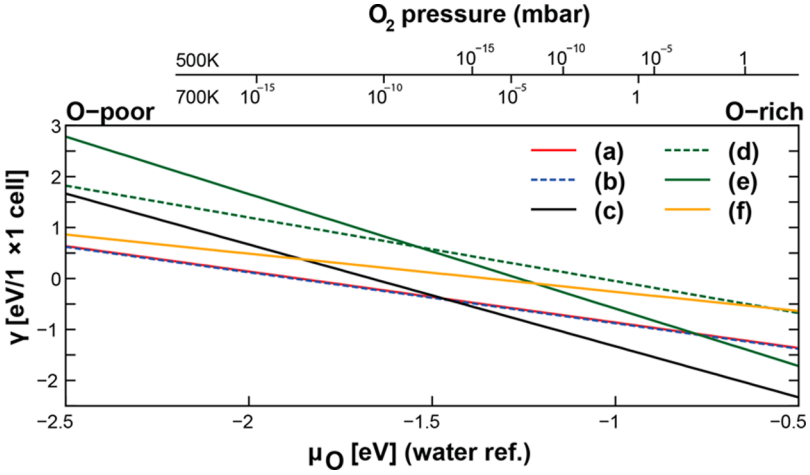

Figure 4. Surface stability per 1 × 1 unit cell of different CoO_x films on the Au(111) surface (A = 7.49 Å^2) as a function of the chemical potential of oxygen. The corresponding structures are shown in Figure 3. The pressure scales for T = 500 K and T = 700 K were constructed according to ref 31.

The cobalt oxide films were adapted to fit the 2 × 2 hexagonal cell of the Au(111) surfaces; *i.e.*, the films are strained to fit the gold support. This allows for determination of the oxide film stability, however, it is not able to capture the moiré pattern as this requires a larger super cell approach. Several possibilities of adsorption of the films on top of the Au surface were investigated. The Co-terminated films prefer adsorption on Au-hollow sites, while oxygen terminated films layer adsorb on top of the Au surface metal atoms. The optimized film structures with indicated layer spacings are shown in Figure 3. Adjusted for the covalent radius of Au (1.34 Å), the heights of the optimized structures are 1.59, 4.36 and 2.68 Å for (a), (b) and (c) structures. This compares very favorably with observed heights of Type A, B and C nanoislands, measured as 1.70 ± 0.2 Å, 4.0 ± 0.2 Å and 2.9 ± 0.2 Å.

The calculated surface stabilities γ (eq 1) of the cobalt oxides films are shown in Figure 4. We find that the Type A and B structures are nearly degenerate and are the most stable structures at low oxygen pressures. At higher oxygen pressures, a more oxidized Type C surface structure is the most stable structure. Depending on the temperature, the calculated structure transition occurs at 10^{-16} to 10^{-6} mbar of oxygen for 500 to 700 K. Lastly, we also test for the stability of 2 ML spinel type structures and Co_2O_3. However, neither of the investigated spinel structures, (d) or (e), nor the Co_2O_3 (f) are stable at the conditions probed by the experiment. The above computationally obtained picture

TABLE 1. Bader Charge and Magnetic Moment Contributions to Co, Au and O Atoms in the Three Most Stable Structures: Type A, B and C

	Co		Au (top layer)	O (near Au)
	Bader charge	mag mom [μ_B]	Bader charge	Bader charge
Type A (AFM)	+1.14	|1.74|	−0.18	–
Type B (AFM)	+1.32 (top) +1.06 (bottom)	|2.11| (top) |2.04| (bottom)	−0.22	–
Type C (FM)	+1.51	0.42	+0.20	−0.92
O−Co−O (no Au)	+1.57	0.80	–	−0.79
Au(111)	–	–	−0.02	–

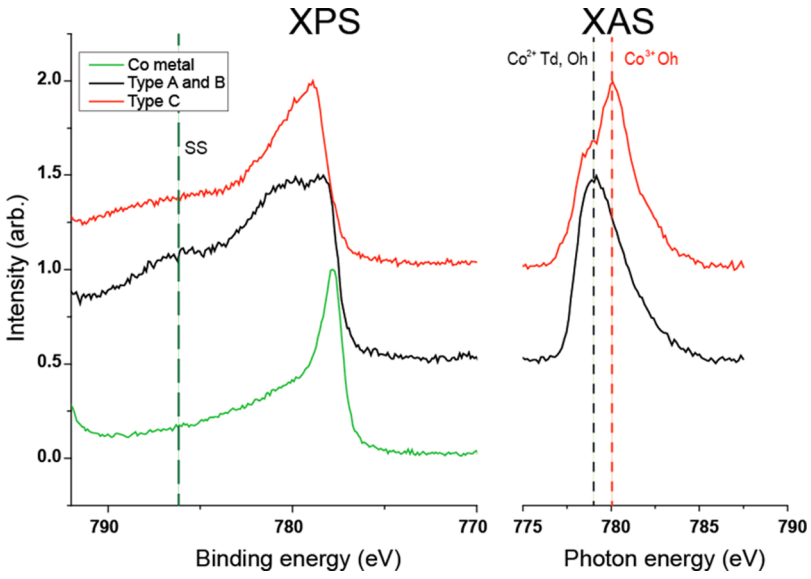

Figure 5. XPS and XAS spectra of the Co $2p_{3/2}$ peak of cobalt oxide nanoislands synthesized at different oxygen pressures. "SS" indicates the position of the shakeup satellite. "Co^{2+} Td,Oh" and "Co^{3+} Oh" indicates the peaks corresponding to tetrahedrally/octahedrally coordinated Co^{2+} and octahedrally coordinated Co^{3+} respectively.

is consistent with our experimental observations of coexistence of Type A and B nanoislands at low oxygen pressure conditions ($p < 10^{-6}$ mbar, $T = 573$ K) and appearance of Type C nanoislands at higher oxygen pressures ($p > 10^{-5}$ mbar, $T = 573$ K).

The obtained magnetic structures reflect the apparent oxidation states of each system and are listed in Table 1. The (a) and (b) structures have high spin magnetic moment [(a): ∼1.7 μ_B per Co site, (b): ∼2.1 μ_B per Co site] and AFM ordering within layers, which is consistent with cobalt in the 2+ oxidation state (for plots of density of states refer to Figure S2 of the Supporting Information). The Au atoms in contact with Co act as weak electron acceptors in the two cases. The more oxidized (c) structure consists of Co sites with lower magnetic moments (∼0.4 μ_B per Co-site) in a FM ordering, which more closely resembles a Co^{3+} character. Contrary to (a) and (b) structures, the charge from Co and Au is transferred toward the intercalating oxygen atoms, with the net result of a small positive charge for the uppermost Au layer. Both spinel structures [(d) and (e)] have metal sites in high magnetic moments (∼2 μ_B per Co site) with the only exception being the octahedrally coordinated Co-sites near the Au interface (e), that show Co-sites with lower magnetic moment (∼0.3 μ_B per Co-site) consistent with a Co^{3+} character.

XPS and XAS Measurements of Co Valency. The cobalt oxidation states predicted by DFT were tested by XPS and XAS spectra acquired on three samples, a mixed A/B synthesis (1×10^{-6} mbar synthesis O_2 pressure), a Type C synthesis (1×10^{-5} mbar synthesis O_2 pressure) and a control of cobalt metal evaporated in UHV conditions (Figure 5). Both the cobalt oxide syntheses show a significant shift to higher binding energies from the cobalt metal peak, confirming that oxidation is complete in both synthesis and no metallic-character cobalt remains. The Type A/B synthesis gave rise to a strong satellite peak and broad main peak in the XPS spectrum and a single peak at low photon energy in the XAS. The Type C synthesis showed much weaker satellite peaks, a narrower main peak and the appearance of a higher energy peak in the XAS spectrum.

The satellite peak and the broad main peak observed in the XPS spectrum of the Type A/B synthesis are indicative of a paramagnetic (high spin) cobalt

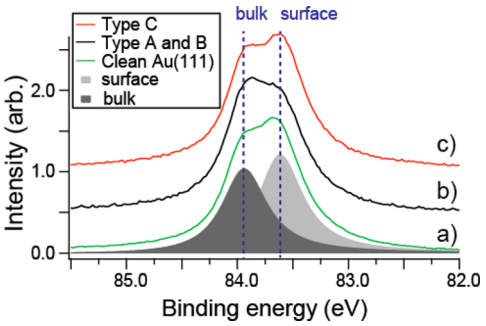

Figure 6. Au $4f_{7/2}$ spectra taken at $h\nu = 110$ eV on (a) a clean Au(111) surface, (b) Type A and B cobalt oxide islands on Au(111) and (c) Type C cobalt oxide islands on Au(111).

species, as the unpaired electrons in the d shell of the cobalt give rise to shakeup excitations (causing the satellite peak) and multiplet splitting of the main peak.[32,33] Conversely, for the Type C synthesis, the XPS spectrum of the Type C synthesis shows strongly suppressed shakeup structure and a narrower main peak suggesting a low spin species. This is fully consistent with the DFT predictions of cobalt valency for the A,B and C structures, with the Type A/B synthesis consisting of high spin Co^{2+} species and the Type C synthesis of low spin Co^{3+}. These spectra are also consistent with bulk reference data, with the spectrum from the Type A/B synthesis qualitatively resembling high spin CoO and the Type C resembling reference data for Co_3O_4 (which is predominantly low spin Co^{3+}) and CoOOH (which is entirely low spin Co^{3+}).[32,33]

XAS spectra are also very sensitive to cobalt valency and coordination and can be used to discriminate between different cobalt oxides.[34,35] Tetrahedral and octahedral Co^{2+} give a broad peak at low photon energy, whereas octahedral Co^{3+} gives rise to a narrower peak at a significantly higher energy (a shift of 2.5 eV). The appearance of a higher energy peak in the XAS spectrum for the Type C synthesis is therefore consistent with the emergence of octahedral Co^{3+} species. The continued presence of a small Co^{2+} peak in this spectrum is attributed to the small amount of Type A islands present at the this pressure and the small number of high Type C islands with an extra layer of Co−O (while the lower cobalt layer is 3+, the upper layer will be in the 2+ state as for Types A and B).

Figure 6 shows Au $4f_{7/2}$ XPS spectra recorded at a photon energy of 110 eV, resulting in a very high surface sensitivity. On the clean Au (111) surface, the peak can be deconvoluted into two components corresponding to the contributions from the surface gold atoms and the bulk gold atoms (Figure 6a). The binding energy shift in the surface component is due to undercoordination of the surface atoms relative to the bulk.[36] When a Type A/B synthesis is made on a gold surface (Figure 6b), a strong reduction in the intensity of the surface component is seen relative to the clean surface. This loss of the surface component implies a strong interaction between the islands and the gold surface, as the surface gold atoms underneath the islands have increased their coordination and become "bulk-like". However, if a Type C synthesis is made on the gold (at the same coverage), no loss of surface component is observed (Figure 6c). This points to a clear structural difference in the islands, as now the underlying gold is not strongly interacting with the islands, and retains its "surface-like" character. The addition of an oxygen layer underneath the cobalt in the islands would explain this change in interaction strength—as this extra oxygen is likely to bind much more strongly to the cobalt and only weakly interact with the gold.

CONCLUSIONS

In summary, we demonstrate based on a combination of experimental and computational findings that the gold/nanoisland interface is central in defining the properties of the cobalt oxide nanoislands. Three distinct types of cobalt oxide nanoislands are observed, two under an oxygen-poor and one under an oxygen-rich environment. For the latter charge transfer from the metal substrate and a change in cobalt valency from 2+ to 3+ stabilizes an extra oxygen layer at the metal/island interface, as has been observed for ultrathin oxides on other metal supports (for example FeO on Pt[28] and CoO on Ir(100)[37]). The degree of charge transfer stabilization is dependent on both the metal support and the oxide chosen and has important implications for the structure's reactivity. In the case of cobalt oxide on gold, it offers a potential explanation for the promotional effect of Au on cobalt oxide catalysts, namely the stabilization of highly active oxygen at the Au/Co oxide interface. In addition, the system of supported ultrathin cobalt oxide nanoislands could be of interest as a catalyst in its own right as part of an emerging new class of catalytic materials, as has been demonstrated for other ultrathin film systems.[28,29,38,39] Finally, we emphasize that the Type C island's structure is identical to that of a single layer of β-CoOOH, reported as the active phase for electrochemical water oxidation[3,4] (*i.e.*, an O−Co−O trilayer), and as such, the study of water's interaction with this structure could yield valuable insight into the nature of the active sites of this important catalytic material.

METHODS

Clean and flat Au(111) surfaces were obtained by cycles of Ar ion sputtering and subsequent annealing. Submonolayer amounts of cobalt were deposited onto the crystal using an electron beam evaporator. The crystal was held at a slightly elevated temperature of 380 K during deposition. For STM

analysis, the same evaporation conditions were used, resulting in a coverage of ~15% ML cobalt oxide. To increase signal-to-noise ratio in XPS analysis, the cobalt coverage was increased such that ~30% ML cobalt oxide was formed (kept constant for all XPS measurements). Deposition of Co was done in an oxygen environment and the sample was subsequently postannealed at 573 K in the same oxygen environment for 15 min. The oxygen pressure at the sample was varied between 1×10^{-6} – 1×10^{-5} mbar.

All analysis was performed under UHV conditions (10^{-10} mbar or better). STM analysis was performed in UHV using a home-built "Aarhus" type STM capable of high speed, atomic-resolution imaging on a routine basis.[40] XPS and XAS analysis was carried out at the I311 beamline at the MAX IV Laboratory.[41] All spectra were recorded at normal emission and photon energies of 110 and 1000 eV were used for acquisition of the Au 4f and Co 2p spectra, respectively. All spectra are calibrated to the Fermi edge and a polynomial background was removed. The Co 2p XAS experiments were performed in Auger yield mode and the photon energy scale was calibrated by recording Au 4f in half and second order mode.

Density functional theory (DFT) calculations have been performed within the Vienna ab initio simulation package[42,43] (VASP) using the projector augmented wave (PAW) potentials.[44] Similar to the study of CoO(111) on Ir(100),[11] we adapted the Perdew–Burke–Ernzerhof[45] (PBE) exchange-correlation functional together with the Hubbard-U approach of Dudarev[46] with a fixed value of $U - J = U_{\mathrm{eff}} = 1$ eV for the localized *d*-electrons of the Co atoms (DFT+U). This value of U_{eff} was shown to be the best compromise between an accurate description of structural and electronic properties (see also SI for additional electronic description). In all calculations, we have employed a 400 eV energy cutoff, 1600 eV density cutoff, and $8 \times 8 \times 8$ Monkhorst–Pack type *k*-point mesh for a $(1 \times 1 \times 1)$ bulk unit cell and a $4 \times 4 \times 1$ gamma centered *k*-point mesh for the (2×2) surfaces. The CoO structures were placed on-top of three layers of Au(111) of which the bottom two layers were fixed at bulk equilibrium positions, and 16 Å of vacuum was used to separate the Au layers. The structures were relaxed with the maximum force threshold of 0.05 eV/Å subject to small dipole corrections.

To model the stability of the films under different synthesis and operating conditions, we compared the relative thermodynamic surface stability of these structures by calculating the surface free energy γ per single surface area *A* as

$$\gamma = (G_{\mathrm{Co}_x\mathrm{O}_y/\mathrm{Au}(111)} - G_{\mathrm{Au}(111)} - N_{\mathrm{CoO}}\mu_{\mathrm{CoO}} - N_{\mathrm{Co}}\mu_{\mathrm{Co}} - N_{\mathrm{O}}\mu_{\mathrm{O}})/A \quad (1)$$

where $G_{\mathrm{Co}_x\mathrm{O}_y/\mathrm{Au}(111)}$ and $G_{\mathrm{Au}(111)}$ are free energies of the slabs with and without cobalt oxide on top of Au(111) with subtracted energy contributions of N_{CoO} complete CoO bulk units and remaining N_{Co} of cobalt and N_{O} of oxygen surface atoms of the slab. This approach allows for comparison of structures of different thickness and stoichiometry. The free energies of the slabs are approximated by their total energies and the chemical potentials, μ_{CoO} and μ_{Co}, are referenced to total energies of the most stable bulk phases, which were found to be bulk RS CoO ($\mu_{\mathrm{CoO}} = E^{\mathrm{total}}_{\mathrm{CoO}}$) and that of metallic bulk Co ($\mu_{\mathrm{Co}} = E^{\mathrm{total}}_{\mathrm{Co}}$) (see also Supporting Information). The chemical potential of oxygen, for any given temperature *T* and pressure *p*, is bounded by the formation energy of bulk RS CoO (oxygen poor) and half of the total energy of an O_2 molecule (oxygen rich) as $E^{\mathrm{free}}_{\mathrm{CoO}} < \mu_{\mathrm{O}}(p,T) - 1/2E_{\mathrm{O}_2}{}^{\mathrm{total}} < 0$. Because of the well-known inaccuracy of $E_{\mathrm{O}_2}{}^{\mathrm{total}}$ within our PBE-DFT approach, higher accuracy is achieved by referencing $E_{\mathrm{O}_2}{}^{\mathrm{total}}$ relative to 2×1.23 eV thermodynamic equilibrium of water and hydrogen gas as $E_{\mathrm{O}_2}{}^{\mathrm{total}} = E_{\mathrm{H}_2\mathrm{O}}{}^{\mathrm{total}} - E_{\mathrm{H}_2}{}^{\mathrm{total}} - 2.506$ eV, which also includes ZPE corrections.[47] Lastly, for a fixed temperature, the correspondence between oxygen chemical potential and oxygen pressure is established following the procedure of Reuter and Scheffler.[31]

Conflict of Interest: The authors declare no competing financial interest.

Acknowledgment. The iNANO group acknowledges support from the Lundbeck Foundation and the European Research Council (ERC Grant no. 239834 (OxideSynergy)). We also acknowledge the Nordforsk network "An interdisciplinary approach to atomistic design of new catalysts" and COST Action CM1104 "Reducible metal oxides". Support from the U.S. Department of Energy Office of Basic Energy Science to the SUNCAT Center for Interface Science and Catalysis is gratefully acknowledged.

Supporting Information Available: Further details of computational methodology and projected density of states for bulk CoO and the three experimentally observed structures (Types A, B and C). This material is available free of charge *via* the Internet at http://pubs.acs.org.

REFERENCES AND NOTES

1. Liao, L.; Zhang, Q.; Su, Z.; Zhao, Z.; Wang, Y.; Li, Y.; Lu, X.; Wei, D.; Feng, G.; Yu, Q.; *et al.* Efficient Solar Water-Splitting Using a Nanocrystalline CoO Photocatalyst. *Nat. Nanotechnol.* **2014**, *9*, 69–73.
2. Rosen, J.; Hutchings, G. S.; Jiao, F. Ordered Mesoporous Cobalt Oxide as Highly Efficient Oxygen Evolution Catalyst. *J. Am. Chem. Soc.* **2013**, *135*, 4516.
3. Bajdich, M.; García-Mota, M.; Vojvodic, A.; Nørskov, J. K.; Bell, A. T. Theoretical Investigation of the Activity of Cobalt Oxides for the Electrochemical Oxidation of Water. *J. Am. Chem. Soc.* **2013**, *135*, 13521–13530.
4. Friebel, D.; Bajdich, M.; Yeo, B. S.; Louie, M. W.; Miller, D. J.; Sanchez Casalongue, H.; Mbuga, F.; Weng, T.-C.; Nordlund, D.; Sokaras, D.; *et al.* On the Chemical State of Co Oxide Electrocatalysts During Alkaline Water Splitting. *Phys. Chem. Chem. Phys.* **2013**, *15*, 17460–17467.
5. Yeo, B. S.; Bell, A. T. Enhanced Activity of Gold-Supported Cobalt Oxide for the Electrochemical Evolution of Oxygen. *J. Am. Chem. Soc.* **2011**, *133*, 5587–5593.
6. Song, F.; Hu, X. Exfoliation of Layered Double Hydroxides for Enhanced Oxygen Evolution Catalysis. *Nat. Commun.* **2014**, *5*, 4477.
7. Gorlin, Y.; Chung, C.-J.; Benck, J. D.; Nordlund, D.; Seitz, L.; Weng, T.-C.; Sokaras, D.; Clemens, B. M.; Jaramillo, T. F. Understanding Interactions between Manganese Oxide and Gold That Lead to Enhanced Activity for Electrocatalytic Water Oxidation. *J. Am. Chem. Soc.* **2014**, *136*, 4920–4926.
8. Helveg, S.; Lauritsen, J. V.; Lægsgaard, E.; Stensgaard, I.; Nørskov, J. K.; Clausen, B. S.; Topsøe, H.; Besenbacher, F. Atomic-Scale Structure of Single-Layer MoS_2 Nanoclusters. *Phys. Rev. Lett.* **2000**, *84*, 951–954.
9. Gong, J. Structure and Surface Chemistry of Gold-Based Model Catalysts. *Chem. Rev.* **2011**, *112*, 2987–3054.
10. Heinz, K.; Hammer, L. Epitaxial Cobalt Oxide Films on Ir(100)—the Importance of Crystallographic Analyses. *J. Phys.: Condens. Matter* **2013**, *25*, 173001.
11. Tröppner, C.; Schmitt, T.; Reuschl, M.; Hammer, L.; Schneider, M. A.; Mittendorfer, F.; Redinger, J.; Podloucky, R.; Weinert, M. Incommensurate Moiré Overlayer with Strong Local Binding: CoO(111) Bilayer on Ir(100). *Phys. Rev. B: Condens. Matter Mater. Phys.* **2012**, *86*, 235407.
12. Ebensperger, C.; Gubo, M.; Meyer, W.; Hammer, L.; Heinz, K. Substrate-Induced Structural Modulation of a CoO(111) Bilayer on Ir(100). *Phys. Rev. B: Condens. Matter Mater. Phys.* **2010**, *81*, 235405.
13. Gragnaniello, L.; Barcaro, G.; Sementa, L.; Allegretti, F.; Parteder, G.; Surnev, S.; Steurer, W.; Fortunelli, A.; Netzer, F. P. The Two-Dimensional Cobalt Oxide (9×2) Phase on Pd(100). *J. Chem. Phys.* **2011**, *134*, 184706–184708.
14. De Santis, M.; Buchsbaum, A.; Varga, P.; Schmid, M. Growth of Ultrathin Cobalt Oxide Films on Pt(111). *Phys. Rev. B: Condens. Matter Mater. Phys.* **2011**, *84*, 125430.
15. Sebastian, I.; Heiler, M.; Meinel, K.; Neddermeyer, H. Growth of Epitaxial Layers of Co and CoO on Au(111). *Appl. Phys. A: Mater. Sci. Process.* **1998**, *66*, S525–S528.
16. Li, M.; Altman, E. I. Cluster-Size Dependent Phase Transition of Co Oxides on Au(111). *Surf. Sci.* **2014**, *619*, L6–L10.
17. Li, M.; Altman, E. I. Shape, Morphology, and Phase Transitions During Co Oxide Growth on Au(111). *J. Phys. Chem. C* **2014**, *118*, 12706–12716.

18. Meyer, W.; Biedermann, K.; Gubo, M.; Hammer, L.; Heinz, K. Surface Structure of Polar Co_3O_4 (111) Films Grown Epitaxially on Ir(100)-(1 × 1). *J. Phys.: Condens. Matter* **2008**, *20*, 265011.
19. Rasmussen, M. K.; Meinander, K.; Besenbacher, F.; Lauritsen, J. V. Noncontact Atomic Force Microscopy Study of the Spinel $MgAl_2O_4$(111) Surface. *Beilstein J. Nanotechnol.* **2012**, *3*, 192–197.
20. Tersoff, J.; Hamann, D. R. Theory of the Scanning Tunneling Microscope. *Phys. Rev. B: Condens. Matter Mater. Phys.* **1985**, *31*, 805–813.
21. Yankowitz, M.; Xue, J.; Cormode, D.; Sanchez-Yamagishi, J. D.; Watanabe, K.; Taniguchi, T.; Jarillo-Herrero, P.; Jacquod, P.; LeRoy, B. J. Emergence of Superlattice Dirac Points in Graphene on Hexagonal Boron Nitride. *Nat. Phys.* **2012**, *8*, 382–386.
22. Sun, Y.-N.; Giordano, L.; Goniakowski, J.; Lewandowski, M.; Qin, Z.-H.; Noguera, C.; Shaikhutdinov, S.; Pacchioni, G.; Freund, H.-J. The Interplay between Structure and Co Oxidation Catalysis on Metal-Supported Ultrathin Oxide Films. *Angew. Chem., Int. Ed.* **2010**, *49*, 4418–4421.
23. Weiss, W.; Ranke, W. Surface Chemistry and Catalysis on Well-Defined Epitaxial Iron-Oxide Layers. *Prog. Surf. Sci.* **2002**, *70*, 1–151.
24. Deng, X.; Yao, K.; Sun, K.; Li, W.-X.; Lee, J.; Matranga, C. Growth of Single- and Bilayer ZnO on Au(111) and Interaction with Copper. *J. Phys. Chem. C* **2013**, *117*, 11211–11218.
25. Risbud, A. S.; Snedeker, L. P.; Elcombe, M. M.; Cheetham, A. K.; Seshadri, R. Wurtzite CoO. *Chem. Mater.* **2005**, *17*, 834–838.
26. Meyer, W.; Hock, D.; Biedermann, K.; Gubo, M.; Müller, S.; Hammer, L.; Heinz, K. Coexistence of Rocksalt and Wurtzite Structure in Nanosized CoO Films. *Phys. Rev. Lett.* **2008**, *101*, 016103.
27. Roy, S.; Meyerheim, H. L.; Mohseni, K.; Tian, Z.; Sander, D.; Hoffmann, M.; Adeagbo, W.; Ernst, A.; Hergert, W.; Felici, R.; *et al.* X-Ray Analysis of Wurtzite-Type CoO(111) Films on Ir(001): Correlation of Structure, Stress, Electronic, and Magnetic Properties. *Phys. Rev. B: Condens. Matter Mater. Phys.* **2014**, *89*, 165428.
28. Zeuthen, H.; Kudernatsch, W.; Peng, G.; Merte, L. R.; Ono, L. K.; Lammich, L.; Bai, Y.; Grabow, L. C.; Mavrikakis, M.; Wendt, S.; *et al.* Structure of Stoichiometric and Oxygen-Rich Ultrathin FeO(111) Films Grown on Pd(111). *J. Phys. Chem. C* **2013**, *117*, 15155–15163.
29. Giordano, L.; Lewandowski, M.; Groot, I. M. N.; Sun, Y. N.; Goniakowski, J.; Noguera, C.; Shaikhutdinov, S.; Pacchioni, G.; Freund, H. J. Oxygen-Induced Transformations of an FeO(111) Film on Pt(111): A Combined DFT and STM Study. *J. Phys. Chem. C* **2010**, *114*, 21504–21509.
30. Kresse, G.; Surnev, S.; Ramsey, M. G.; Netzer, F. P. First-Principles Calculations for V_xO_y Grown on Pd(111). *Surf. Sci.* **2001**, *492*, 329–344.
31. Reuter, K.; Scheffler, M. Composition, Structure, and Stability of RuO_2(110) as a Function of Oxygen Pressure. *Phys. Rev. B: Condens. Matter Mater. Phys.* **2001**, *65*, 035406.
32. Chuang, T. J.; Brundle, C. R.; Rice, D. W. Interpretation of the X-Ray Photoemission Spectra of Cobalt Oxides and Cobalt Oxide Surfaces. *Surf. Sci.* **1976**, *59*, 413–429.
33. Casella, I. G.; Guascito, M. R. Anodic Electrodeposition of Conducting Cobalt Oxyhydroxide Films on a Gold Surface. XPS Study and Electrochemical Behaviour in Neutral and Alkaline Solution. *J. Electroanal. Chem.* **1999**, *476*, 54–63.
34. Morales, F.; de Groot, F. M. F.; Glatzel, P.; Kleimenov, E.; Bluhm, H.; Hävecker, M.; Knop-Gericke, A.; Weckhuysen, B. M. *In Situ* X-Ray Absorption of Co/Mn/TiO_2 Catalysts for Fischer–Tropsch Synthesis. *J. Phys. Chem. B* **2004**, *108*, 16201–16207.
35. Papaefthimiou, V.; Dintzer, T.; Dupuis, V.; Tamion, A.; Tournus, F.; Hillion, A.; Teschner, D.; Hävecker, M.; Knop-Gericke, A.; Schlögl, R.; *et al.* Nontrivial Redox Behavior of Nanosized Cobalt: New Insights from Ambient Pressure X-Ray Photoelectron and Absorption Spectroscopies. *ACS Nano* **2011**, *5*, 2182–2190.
36. Heimann, P.; van der Veen, J. F.; Eastman, D. E. Structure-Dependent Surface Core Level Shifts for the Au(111), (100), and (110) Surfaces. *Solid State Commun.* **1981**, *38*, 595–598.
37. Gubo, M.; Ebensperger, C.; Meyer, W.; Hammer, L.; Heinz, K. Structural Elements in the Oxidation Process of a Single Cobalt Layer on Ir(100)-(1 × 1). *Phys. Rev. B: Condens. Matter Mater. Phys.* **2011**, *83*, 075435.
38. Fu, Q.; Li, W.-X.; Yao, Y.; Liu, H.; Su, H.-Y.; Ma, D.; Gu, X.-K.; Chen, L.; Wang, Z.; Zhang, H.; *et al.* Interface-Confined Ferrous Centers for Catalytic Oxidation. *Science* **2010**, *328*, 1141–1144.
39. Martynova, Y.; Shaikhutdinov, S.; Freund, H.-J. Co Oxidation on Metal-Supported Ultrathin Oxide Films: What Makes Them Active? *ChemCatChem* **2013**, *5*, 2162–2166.
40. Walton, A. S.; Lauritsen, J. V.; Topsøe, H.; Besenbacher, F. MoS_2 Nanoparticle Morphologies in Hydrodesulfurization Catalysis Studied by Scanning Tunneling Microscopy. *J. Catal.* **2013**, *308*, 306–318.
41. Nyholm, R.; Andersen, J. N.; Johansson, U.; Jensen, B. N.; Lindau, I. Beamline I311 at Max-Lab: A VUV/Soft X-Ray Undulator Beamline for High Resolution Electron Spectroscopy. *Nucl. Instrum. Methods Phys. Res., Sect. A* **2001**, *467–468*, 520–524.
42. Kresse, G.; Furthmüller, J. Efficiency of *Ab-Initio* Total Energy Calculations for Metals and Semiconductors Using a Plane-Wave Basis Set. *Comput. Mater. Sci.* **1996**, *6*, 15–50.
43. Kresse, G.; Hafner, J. *Ab Initio* Molecular Dynamics for Liquid Metals. *Phys. Rev. B: Condens. Matter Mater. Phys.* **1993**, *47*, 558–561.
44. Kresse, G.; Joubert, D. From Ultrasoft Pseudopotentials to the Projector Augmented-Wave Method. *Phys. Rev. B: Condens. Matter Mater. Phys.* **1999**, *59*, 1758–1775.
45. Perdew, J. P.; Burke, K.; Ernzerhof, M. Generalized Gradient Approximation Made Simple. *Phys. Rev. Lett.* **1996**, *77*, 3865–3868.
46. Dudarev, S. L.; Botton, G. A.; Savrasov, S. Y.; Humphreys, C. J.; Sutton, A. P. Electron-Energy-Loss Spectra and the Structural Stability of Nickel Oxide: An LSDA+U Study. *Phys. Rev. B: Condens. Matter Mater. Phys.* **1998**, *57*, 1505–1509.
47. Ebensperger, C.; Meyer, B. First-Principles Study of the Reconstruction and Hydroxylation of the Polar NiO(111) Surface. *Phys. Status Solidi B* **2011**, *248*, 2229–2241.